JGR Space Physics

RESEARCH ARTICLE
10.1029/2019JA026836

Electron Dispersion and Parallel Electron Beam Observed Near the Separatrix

Shi-Chen Bai[1,2], Quanqi Shi[1], Qiu-Gang Zong[3], Xiaogang Wang[4], Anmin Tian[1], Alexander W. Degeling[1], Chao Yue[2], I. Jonathan Rae[5], Zu-Yin Pu[3], and Suiyan Fu[3]

[1]Shandong Provincial Key Laboratory of Optical Astronomy and Solar-Terrestrial Environment, School of Space Science and Physics, Shandong University, Weihai, China, [2]Department of Atmospheric and Oceanic Sciences, University of California, Los Angeles, CA, USA, [3]School of Earth and Space Sciences, Peking University, Beijing, China, [4]Department of Physics, Harbin Institute of Technology, Harbin, China, [5]Mullard Space Science Laboratory, Space and Climate Physics, University College London, Dorking, UK

Key Points:
- Rapid dispersion is observed at the electron edge, indicating that electrons are decoupled from the magnetic field close to separatrix
- The width of the electron diffusion region on the magnetosheath side is estimated using in situ observations
- A parallel electron beam is observed outside of the separatrix in the magnetosheath for the first time

Supporting Information:
- Supporting Information S1
- Figure S1

Correspondence to:
Q. Shi,
sqq@pku.edu.cn

Citation:
Bai, S.-C., Shi, Q., Zong, Q.-G., Wang, X., Tian, A., Degeling, A. W., et al. (2019). Electron dispersion and parallel electron beam observed near the separatrix. *Journal of Geophysical Research: Space Physics*, *124*, 7494–7504. https://doi.org/10.1029/2019JA026836

Received 14 APR 2019
Accepted 16 AUG 2019
Accepted article online 29 AUG 2019
Published online 9 SEP 2019

Abstract The separatrix region is the region between the separatrix and the reconnection jet. Due to the *E*×*B* drift and velocity filter effect in which high-energy particles with high parallel speed can be seen prior to low-energy particles along the field line, electrons are separated from ions. The electron dynamics in this region is of interest; however it has not been studied in detail, because of the insufficient resolution of plasma data. We present a slow separatrix crossing event observed by Magnetospheric Multiscale (MMS) satellite constellation on 1 January 2016, from the magnetosheath side with high-resolution burst mode data. The electron edge and ion edge are clearly distinguished in the separatrix region. Two types of electron dispersion, one with a short duration (~0.3 s) and the other with a longer duration (~13 s) were detected between the electron and ion edges. The rapid dispersion (with small time scale) is mainly in the parallel direction, which might originate from a thin layer with non-frozen-in electrons close to the separatrix. The gradual (long time scale) dispersion is seen from parallel to perpendicular directions, which comes from the *E*×*B* drift of a curved D-shape distribution of electrons. The width of the electron diffusion region on the magnetosheath side is estimated based on MMS observation. The observation also reveals an unexpected parallel electron beam outside of the electron edge. Wave-particle interaction or parallel potential in the inflow region may be responsible for the generation of this electron population.

Plain Language Summary Magnetic reconnection is a process commonly occurred at the Sun, the dayside magnetopause, and in the magnetotail that changes magnetic topology, and converts electromagnetic energy into plasma kinetic and thermal energies. Due to the different parallel velocities of the particles and field line convection, electrons are separated from ions, and this creates the electron edge and ion edge in the separatrix region. These separations downstream of the X-line widen the distance in the convection direction between the field lines involved in the reconnection. This, in turn, makes it easier for the satellite to observe the changes in the magnetic field topology and electronic dynamics during magnetic reconnection. However, high-resolution satellite data are still required for the observation of the separatrix region in the downstream. The unprecedented high temporal and spatial resolution measurements of the Magnetospheric Multiscale (MMS) mission provide a unique opportunity to perform such studies. By analyzing the magnetic field and plasma data from MMS, this study has revealed the field line topology and electron dynamics between the electron and ion edges. Possible generation mechanisms based on the electron dynamics are also discussed in this paper.

1. Introduction

Magnetic reconnection is a fundamental process in plasma physics. During this process, the field topology changes and electromagnetic energy is converted into plasma kinetic and thermal energies (Birn et al., 2001; Lau & Finn, 1990). The energy conversion mainly occurs on the small scale (ion inertial length scale and electron inertial length scale), which historically has been difficult to investigate using the available limited time resolution data from in situ observations. The separations between the field lines involved in the reconnection in the convection direction are wider in the separatrix region in the downstream of the X-line. Electrons are decoupled from ions in this region due to their different velocities along field lines and their *E*×*B* drift. As a result, the electron edge, where the electrons accelerated by reconnection, is first observed

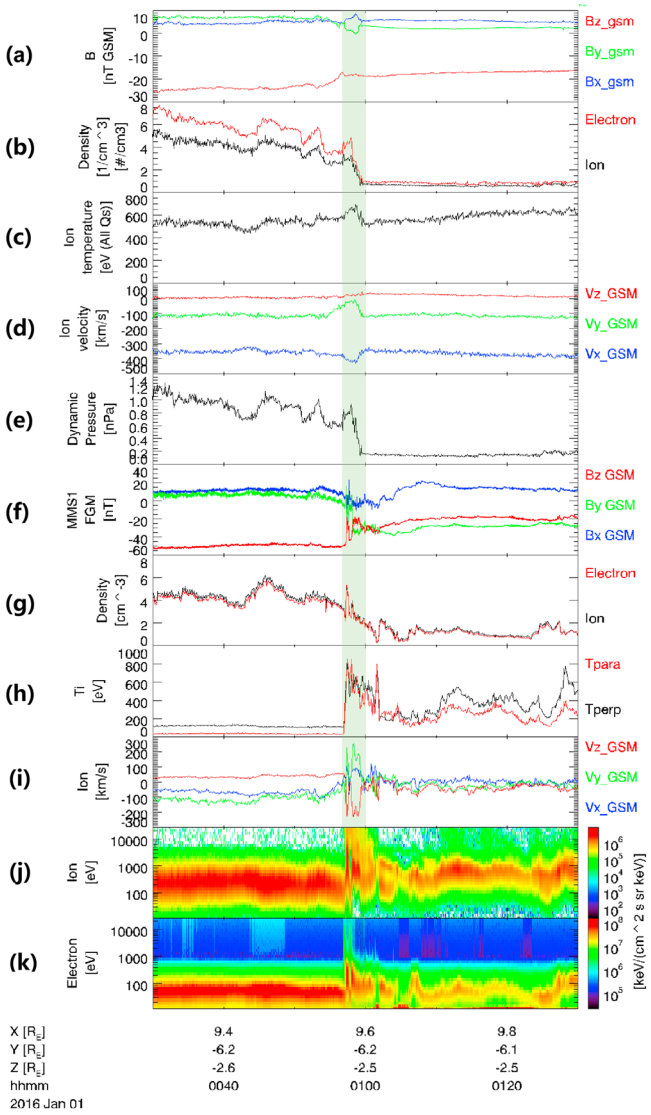

Figure 1. Overview of the case in geocentric solar magnetospheric (GSM) coordinate. Blue/green/red line for *X*/*Y*/*Z* component. The green shaded region is the interval of the Magnetospheric Multiscale (MMS) burst mode. Themis-B observation of the (a) magnetic field, (b) ion (black) and electron (red) number density, (c) ion temperature, (d) ion velocity, and (e) dynamic pressure in the solar wind. MMS fast mode observation of the (f) magnetic field, (g) number density of ion (black) and electron (red), (h) ion temperature in parallel (red) and perpendicular (black) direction, (i) ion velocity, (j) omnidirectional ion energy flux, and (k) omnidirectional electron energy flux. Themis-B data are shifted based on the solar wind and the separation between MMS and Themis-B in GSM *X* direction.

closer to the separatrix, and the ion edge is then observed close to the reconnection jet (Gosling et al., 1990; Onsager et al., 1990). The ion edge is characterized by the arrival of high energy ions accelerated by reconnection. Energy dispersion of particles can be identified clearly at these edges far from the X-line. The position of X-line can therefore be obtained by analyzing electron and ion energy dispersion. Both of these edges are a spatial effect and require a sustained source to maintain, which are one of the observational characteristics of steady-state reconnection (Trattner et al., 2015). The heating and acceleration processes of particles in the source region can be inferred from these electron and ion edges in the downstream region, which will help us better understand the energy conversion in magnetic reconnection. However, to date, a detailed investigation of the source region of dispersed particles has yet to be carried out. For example, whether or not the particles involved in the dispersion come from the diffusion region is still unclear. The correspondence of electron and ion edges between the vicinity of the reconnection and the downstream has not been established, which is important for understanding the global process of magnetic reconnection.

Subregions within the separatrix region, such as the density cavity, electron phase space holes, have been identified in previous studies (Chen et al., 2005; Khotyaintsev et al., 2006; Mozer et al., 2016; Retinò et al., 2006). Øieroset et al. (2015) found that the field lines between the electron edge and ion edge on the magnetospheric side are connected to the magnetosheath by analyzing the electron dynamics in that region, which indicate that the field lines in this region have undergone reconnection. By comparing the velocity of $E\times B$ drift and the perpendicular velocity of electrons in iPic3D simulations, Lapenta et al. (2015) found that the electrons are not frozen-in close to the separatrix while far from the X-line. However, due to a lack of high cadence electron measurements, whether or not the frozen-in condition applies for electrons in this region has not been confirmed by in-situ observations, and the location where electrons start to become magnetized remains unclear. Furthermore, the study of the downstream electron dynamics may provide a way to remote sense the width of the electron diffusion region (EDR), which is crucial for quantitative analysis of the reconnection rate.

The Magnetospheric Multiscale (MMS; Burch et al., 2015) provides unprecedented of high-resolution plasma data (30 ms for electrons and 150 ms for ions in the burst mode), which gives a good opportunity to investigate the electron dynamics, and further field line topology can be analyzed based on the plasma observation. We present a case in which MMS slowly crosses the separatrix region over an interval between 00:56:45 UT and 00:57:40 UT on 1 January 2016. Two new features of electron spectrum are observed: (i) two types of dispersion near the electron edge and (ii) a parallel electron beam ahead of the electron edge.

2. Observations

In this paper, MMS observations from several instruments are used: magnetic field B data from the Fluxgate Magnetometer (Russell et al., 2016), plasma data from the Fast Plasma Investigation (FPI; Pollock et al., 2016), Fly's Eye Energetic Particle Spectrometer (FEEPS; Blake et al., 2015), and Energetic Ion Spectrometer (EIS; Mauk et al., 2016), and electric field *E* data from the Electric field Double Probes (EDP; Lindqvist et al., 2016; Ergun et al., 2014). Themis-B (Angelopoulos, 2008), located at (−15.3, −62.3, −14.7) Earth radii (RE; geocentric solar magnetospheric [GSM]), provides the magnetic field

(Auster et al., 2008) and plasma measurements (McFadden et al., 2008) in the solar wind. The data from Themis-B is time-shifted to the MMS location at (9.6, −6.2, −2.5) RE (GSM) based on the solar wind velocity and the separation distance between MMS and Themis B.

2.1. Overview

An overview of this case observed by MMS1 is presented in Figure 1. The solar wind magnetic field and velocity (shown in Figures 1a and 1c, respectively) are stable before and after a clear reduction in ion and electron number density (shown in Figure 1b), which starts from 00:57:55 UT. Prior to this abrupt decrease, the ion and electron density have a more gradual decreasing trend from 6 to 3.5 cm^{-3} for electrons and from 4 to 2.5 cm^{-3} for ions starts from 00:53:30 UT. Due to the solar wind dynamic pressure drop resulting from the density drop observed by Themis-B (shown in Figure 1e), the outflow region is observed twice in the green shaded region. After the solar wind dynamic pressure decrease, the solar wind becomes sub-Alfvénic, which is also observed by the Wind satellite (not shown). The magnetopause velocity is 67.02 km/s × (0.95, −0.01, 0.30; GSM) inferred from timing analysis (Schwartz, 1998). The magnetosheath electron inertial length is $d_{e,\mathrm{Msh}}$ =2.39 km based on MMS observations. However, GSM B_z is shown to stay negative in Figure 1f, indicating that MMS did not cross the magnetopause over this time interval. The energy spectrum of the magnetosheath completely changes in Figures 1j and 1k due to the solar wind becomes sub-Alfvénic after 00:59:00 UT.

2.2. Electron Edge and Ion Edge

The MMS crossed the reconnection jet twice during the time interval corresponding to the solar wind dynamic pressure decrease. In this paper, we focus on the first encounter with the reconnection jet during 00:56:18–00:56:40 UT, which is characterized as a southward reconnection jet of ~300 km/s in Figure 1i. Both ion velocity (−291 km/s) and electron velocity (−259.3 km/s) during this interval are close to the local Alfvén speed (−282.5 km/s). The magnetic field starts to change after the ion edge is encountered, shown in Figures 2a and 2b. A density cavity is shown between the ion edge and reconnection jet in Figure 2c, which is consistent with the previous observation (Retinò et al., 2006). The density is decreased in the second reconnection jet, and the solar wind becomes sub-Alfvénic during this time. A significant enhancement of the ion temperature is found at the ion edge in Figure 2d. A similar enhancement of the electron temperature is observed at the electron edge in Figure 2e. These temperature enhancements are related to the presence of high energy particle in the parallel direction. A large amplitude electric field is observed in Figure 2f close to the electron edge. This electric field could be produced by a two-stream instability between ions and electrons and/or between hot and cold electrons (Hoshino et al., 2001; Retinò et al., 2006) or by density gradients (Graham et al., 2016; Retinò et al., 2006). The southward reconnection jet is observed with large GSM V_z (~300 km/s) in Figure 2g and confirmed by Walén relation (Paschmann et al., 1986) given by equation.

$$v-V_{HT} = \pm\left(\frac{1-\alpha_1}{\mu_0\rho_1}\right)\left[B_2\left(\frac{1-\alpha_2}{1-\alpha_1}\right)-B_1\right] \quad (1)$$

The pressure anisotropy factor is $\alpha=(p_{||}\text{-}p_{\perp})\mu_0/B^2$, where $p_{||}$and $p_{\perp}$ are the plasma pressures parallel and perpendicular to **B.** Suffix 1 refers to the 00:57:45–00:57:55 UT interval when MMS were in the magnetosheath. Suffix 2 refers to the 00:57:18–00:57:40 UT interval when MMS observes the reconnection jet, which is indicated by the blue shaded region in Figure 2. The correlation coefficients are high (R>0.93), and the slopes of the fitted lines (shown in Figure 2l) are close to one.

The electron edge shown in Figure 3d at 00:56:55.8 UT is characterized by an energy dispersion in the accelerated magnetosheath electrons in the parallel direction. The ion edge shown in Figure 3a at 00:57:04 UT is characterized by an energy dispersion of the accelerated ions in the parallel direction. Here we consider that the particles observed by FPI come from the magnetosheath due to an apparent reduction in electron energy flux of the highest energy channel of FPI after the solar wind density drop at 00:57:55 UT (not shown). Higher energy particles coming from the magnetospheric leakage can also be seen at the electron and ion edge separately shown in Figures 2h and 2j. The magnetospheric ions were observed before the ion edge and shown in Figure 2h. These ion populations, mainly with 90-degree pitch angles (not shown), probably come from the large gyroradii of high-energy ions, which are not related to the reconnection. The separatrix

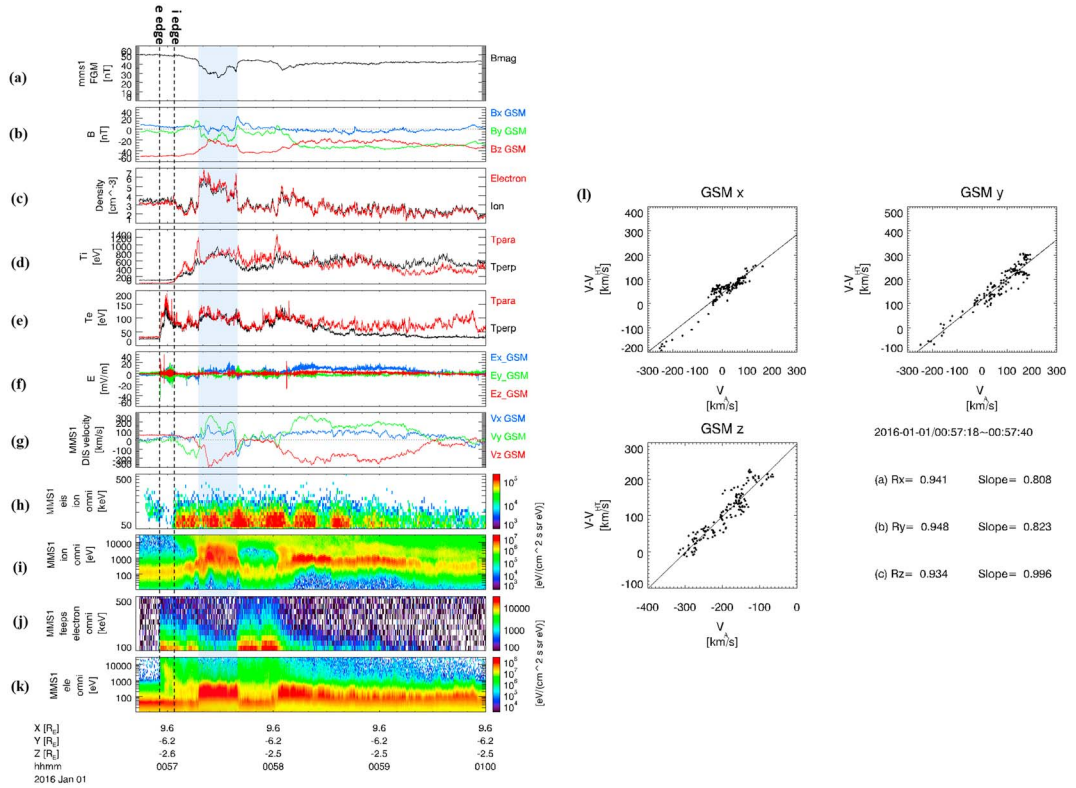

Figure 2. Magnetospheric Multiscale (MMS) 1 burst mode observation in geocentric solar magnetospheric (GSM) coordinate in the 00:56:45–01:00:00 UT interval on 1 January 2016 (a) magnitude of magnetic field, (b) magnetic field, (c) number density of ion (black) and electron (red), (d) temperature of ion in parallel direction (red) and perpendicular direction (black), (e) temperature of electron in parallel direction (red) and perpendicular direction (black), (f) electric field, (g) ion velocity,, (h) omnidirectional ion energy flux (50–500 keV), (i) omnidirectional ion energy flux (10–30,000 eV), (j) omnidirectional electron energy flux (100–500 keV), (k) omnidirectional electron energy flux (10–30,000 eV), (l) Walén test of the blue shaded region (00:56:18–00:56:40 UT). Correlation coefficients (Rx/Ry/Rz) of the velocity change in HT frame cross the magnetosheath separatrix and the local Alfvén speed are shown. The slope of the fitted line is also shown. The electron and ion edge of the reconnection are marked by two dashed line.

is where we see the beginning of magnetic field change and first place to see the plasma accelerated by reconnection (Øieroset et al., 2015). Therefore, in this paper, we consider that the separatrix region starts from the electron edge. Figure 3d shows that magnetosheath electrons with energies below 50 eV disappear from the ion edge, presumably due to field line topology changes.

2.3. Two Types of Electron Dispersion and X-Line Distance

Another thing we noticed in Figure 3d is that two types of electron dispersion start from the separatrix at 00:56:56.8 UT. The long (short) dispersion feature has an ~13s (~0.8s) time scale and ~8.54$d_{i,\ \mathrm{Msh}}$ (~22.43$d_{e,\ \mathrm{Msh}}$) spatial scale. Compared Figures 3e to 3d, the long dispersion starts 0.3s after the short dispersion (~0.8s, 22.43$d_{e,\ \mathrm{Msh}}$), which indicates that the source regions for these two dispersion features are close to each other. Both of these two dispersion features, which have the same energy range, come from the accelerated magnetosheath electrons. Unlike the short dispersion, which can be seen mainly in the parallel direction, the long electron dispersion can be seen, with the same slope, from parallel to perpendicular directions in Figures 4b–4g. We can see that the long dispersion is related to the curved D shape electron distribution shown in Figure 4g.

Using the short electron energy dispersion shown in Figure 3d, we calculate the distance between the X-line and the MMS location based on the following equation.

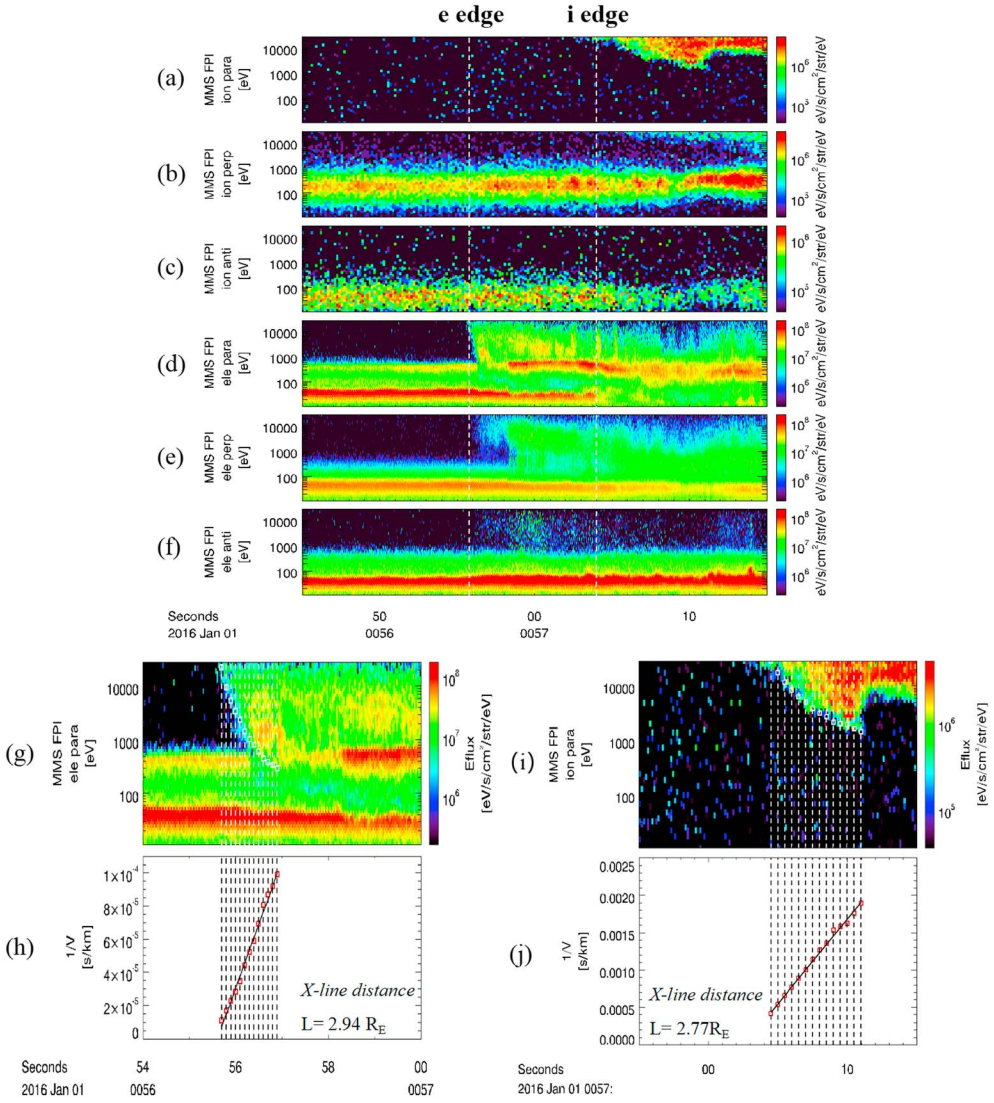

Figure 3. Magnetospheric Multiscale (MMS) 1 observation of energy spectrum of ions moving (a) parallel to the field line, (b) perpendicular to the field line, (c) anti-parallel to the field line, MMS observation of energy spectrum of ions moving (d) parallel to the field line, (e) perpendicular to the field line, (f) antiparallel to the field line, and (g) energy spectrum of electrons moving parallel to the field line. The dispersion is marked by the white squares at the selected time (white dashed line); (h) reciprocal of parallel velocity of the electron marked by the white square in (g). (i) Energy spectrum of ions moving along the field line. The dispersion is marked by the white squares at the selected time (white dashed line). (j) Reciprocal of parallel velocity of the ion marked by the white square in (i). The black dashed lines in (h) and (j) marked the time that we selected to calculate the X-line distance. The black lines in (h) and (j) are linear fitting traces by minimizing the chi-square error statistic. The X-line distance can be calculated by the slope of the black lines.

$$\frac{1}{V_{\text{para}}} = \frac{V_{\text{sc}}}{V_c}\frac{1}{L}(t-t_0) \tag{2}$$

Here we use the reference frame where magnetopause is stationary. V_{para} is the parallel velocity of the selected energy, and relativistic effects are not taken into account considering the low energy range involved. V_c is the convection velocity of field line in the magnetopause reference frame. This is obtained by projecting the plasma velocity observed by FPI into the normal direction and reducing the velocity of magnetopause motion. V_c is 46.30 km/s for electrons and 15.75 km/s for ions. The electron velocity is averaged in the 00:56:55–00:56:57 UT interval. The ion velocity is averaged in the 00:57:00–00:57:13.2 UT interval. V_{sc} is the velocity of MMS. Since the MMS location does not change in the separatrix region, the velocity of V_{sc}

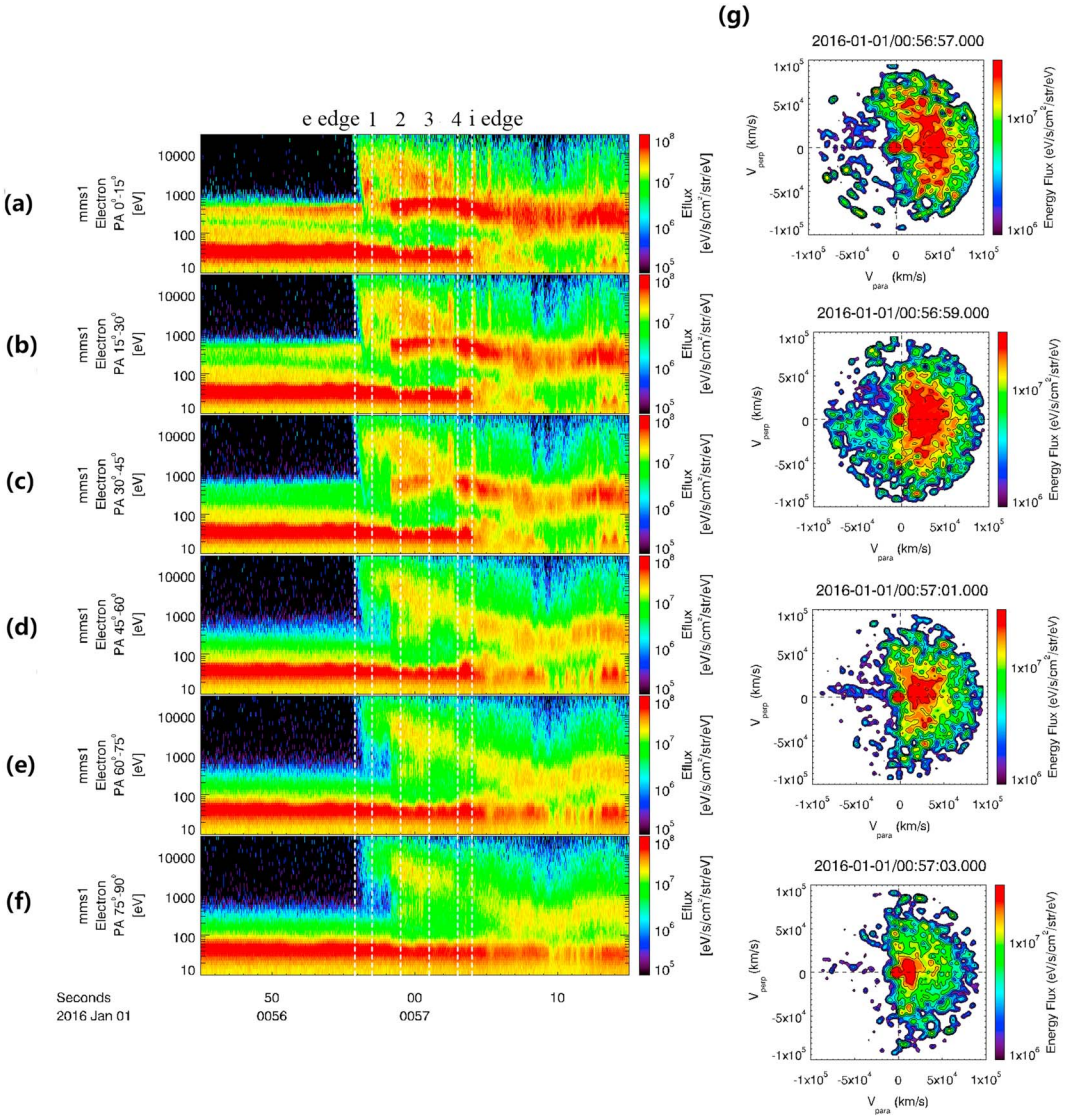

Figure 4. Magnetospheric Multiscale (MMS) 1 burst mode observation of energy flux of electron with pitch angle between (a) 0–15°, (b) 15–30°, (c) 30–45°, (d) 45–60°, (e) 60–75°, and (f) 75–90° in the 00:56:45–00:57:15 interval. (g) Two-dimensional cuts (V_{para} vs V_{perp} [bulk velocity direction]) through the 3-D electron distributions (in units eV/[cm^2 s str eV]) obtained at 1 to 4 marked at (a) from top to bottom during the long dispersion.

is equal to the magnitude of the velocity of the magnetopause (67.02 km/s) in the opposite direction. $\boldsymbol{L}$ is the distance between the X-line and the MMS location in the field line direction. t_0 is the time when the particle leaves the source region.

The calculation result based on the electron energy dispersion are shown in Figures 3g and 3h, and the ion energy dispersion in Figure 3a is also examined using equation (2), and the results are shown in Figures 3i and 3j. According to the calculation based on equation (2), MMS is 2.77–2.94 RE or 173.02–183.63 $d_{i,\,\text{Msh}}$ distance away from the X-line in the parallel direction. The magnetosheath ion inertial length $d_{i,\,\text{Msh}}$ is 102 km in this case.

2.4. Parallel Electron Beam

A parallel electron beam with an energy between 300 to 500 eV is seen for the first time outside of the electron edge in Figures 4a–4c before 00:56:55.8 UT. This parallel electron beam is accelerated close to the electron edge during 00:56:55.8–00:56:57 UT, and the energy range is changed to 1–2 keV and then gradually

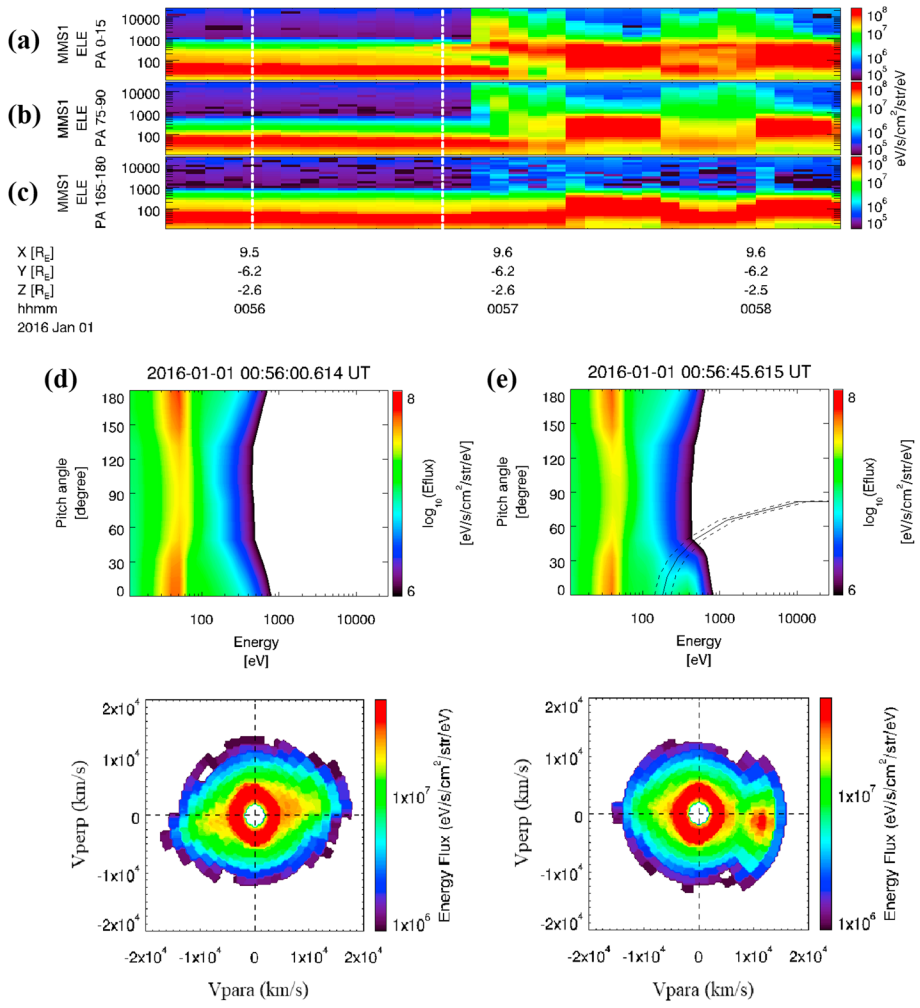

Figure 5. Magnetospheric Multiscale (MMS) 1 fast mode observation of energy flux of electron with pitch angle between (a) 0–15°, (b) 75–90°, and (c) 165–180°. The white dashed line is marked in the (a)–(c). (d) Electron pitch angle distributions obtained at the first white dashed line. The upper panel corresponding to the first time we selected in (a) (first white dashed line) displays the energy flux (eV/s/cm^2/str/eV) as a function of energy and pitch angle. The lower panel shows the two-dimensional cuts through the three-dimensional electron distributions (in units eV/s/cm^2/str/eV) as a function of the velocity perpendicular (y axis) and parallel (x axis) to the magnetic field. (e) Same format as (f) for the second time we selected in (a) (second white dashed line). The curved lines in the upper panel of Figures 5e, given by $\theta = \cos^{-1}[(E_{//}/E)^{1/2}]$, show the contour line of parallel energy $E_{//}$=140 eV (dashed line), 180 eV (solid line), and 230 eV (dashed line).

return to 300–500eV during 00:56:56.3–00:56:56.9 UT. No further acceleration of the parallel electron beam is seen after 00:56:56.9 UT, and the beam becomes thermalized. Figure 4g shows that the parallel electron beam becomes merged with the curved D-shape distribution close to the reconnection jet from 00:57:03 UT shown in Figure 4g.

To clarify that this new electron population does not come from the background magnetosheath, the fast mode data are plotted in Figures 5a–5c. The parallel electron beam starts to appear only ahead of the electron edge from 00:56:45 UT and was not seen in the magnetosheath. Figures 5d and 5e show the electron pitch angle distribution before and after the appearance of the parallel electron beam in detail and indicates that the parallel energy flux of electrons between 140 and 230 eV is decreased and forms a slot between the two dashed lines in the upper panel of Figure 5e. The parallel energy flux of electrons between 300 and 500 eV is increased and forms the parallel electron beam. A cigar-like distribution of the magnetosheath electrons can be seen in the lower panel of Figure 5d before the appearance of the parallel electron beam, which is often considered as the result of Fermi acceleration in the inflow region (Chen et al., 2016). We, therefore, consider

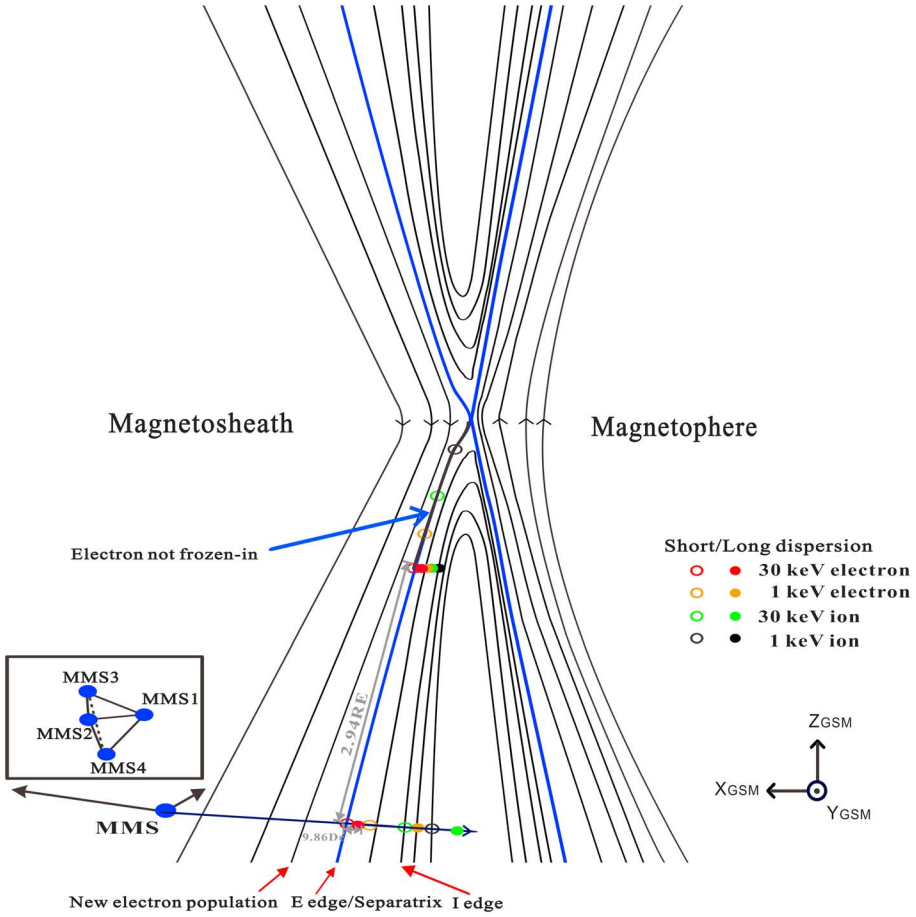

Figure 6. Illustration of the Magnetospheric Multiscale (MMS) cross the separatrix between the 00:56:45 and 00:57:40 UT interval on 1 January 2016. The electron edge/separatrix is marked by the first observation of magnetosheath electrons (red circle) as blue thick line. The ion edge is marked by the first observation of magnetosheath ions (green circle). The short dispersion is illustrated by the red and orange circles. The long dispersion is illustrated by the red and orange dots. A black thin layer close to the separatrix is added to show the region where frozen in condition is broken.

that the combined effect of Fermi acceleration and a field-aligned potential can be a candidate for the generation of the parallel electron beam in the inflow region. This mechanism will be discussed in the next session.

3. Discussions and Conclusions

This study investigates the electron dynamics in the separatrix region using the high-resolution plasma data from MMS. Two types of electron energy dispersion within the same energy range are observed by four satellites in the separatrix region. Both of these dispersions are a spatial effect. The source regions for these two dispersions are close to each other. The short electron dispersion is close to the separatrix, and the electrons involved are mainly in the parallel direction. The long electron dispersion, seen from parallel to perpendicular direction, lasts for ~13s in the separatrix region. We consider that the formation of the long dispersion is related to the D-shape electron distribution, field line convection, and the enhancement of the magnetic field along the field line. Electrons with larger V_{para} can travel further along the field line, while the field line is convected away from X-line by $E \times B$ drift in parallel direction. Thus, the electron cutoff velocity of the D-shape electron distribution close to the X-line decreases from separatrix to reconnection jet. Due to the enhancement of the magnetic field along the field line, the D-shaped electron distribution gradually bends along the field line and becomes crescent-like shape distribution far away from X-line. Combined with these effects, shown in Figure 4g, from top to bottom, the cutoff velocity of the curved D-shaped electron

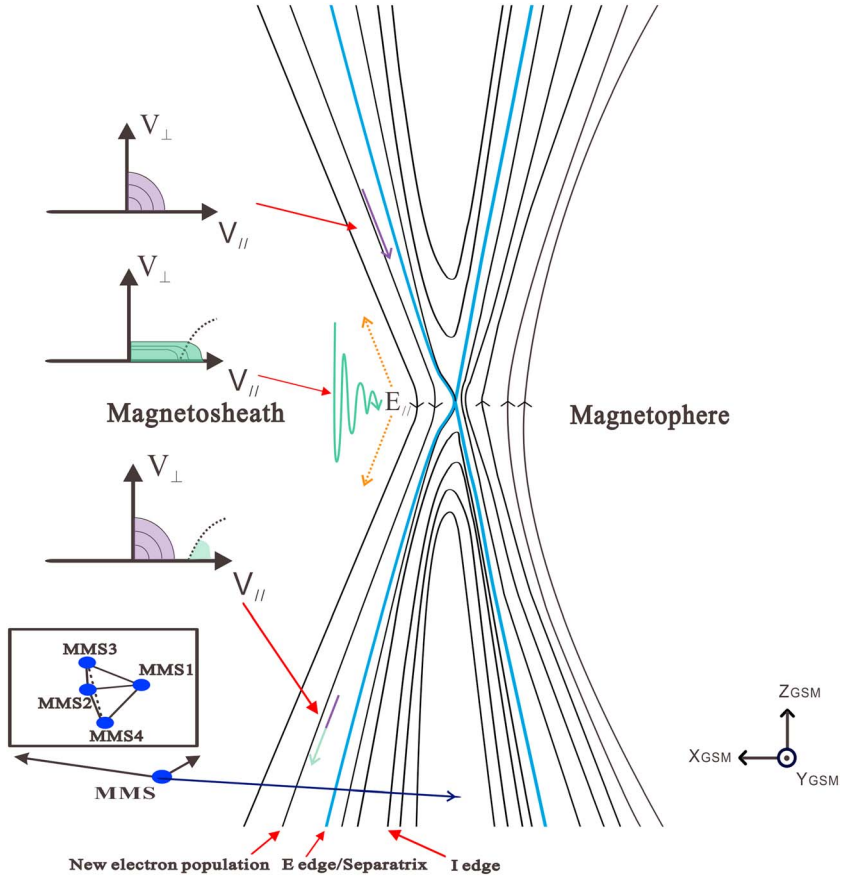

Figure 7. Illustration of the generation of the parallel electron beam. Purple routine for the magnetosheath electrons; green routine for the trapped magnetosheath electrons through Fermi acceleration. The electron edge/separatrix is marked as blue thick line. The dashed line in electron velocity distribution is the boundary between trapped and non-trapping electrons by parallel potentials and magnetic fields. The orange line is the parallel electric field in the trap region.

distribution decreases with the MMS motion away from the electron edge. These phenomena have not been observed previously for electrons, but similar phenomena have been studied for ions. The decrease of the cutoff velocity of the curved D shape ion distribution caused by the $E\times B$ drift has been observed in PIC simulation (Broll et al., 2017; ignoring the effect of wave-particle interactions) and cluster observation (Fuselier et al., 2018). Therefore, both of these two dispersions are caused by the $E\times B$ drift; however, the time for $E\times B$ drift is different. This indicates electrons, marked as different colored-dots in Figure 6, are magnetized close to the X-line resulting in a long dispersion.

In contrast, electrons, marked as different colored-circles in Figure 6, start to have a $E\times B$ drift with the field line far away from the X-line producing a short dispersion. Hence, electrons are not frozen in close to the separatrix away from the X-line marked as a black thin layer in Figure 6, which is consistent with the iPIC3D simulation results [see Lapenta et al., 2015, Figure 4]. The non-frozen-in property of the electrons, which need to be studied in the future, might be related to the magnetic field minima and/or large amplitude of electric field at the electron scale produced by a two-stream instability between ions and electrons and/or between hot and cold electrons (Hoshino et al., 2001; Lapenta et al., 2015; Retinò et al., 2006). We consider it unlikely that these two dispersions are resulting from multiple reconnection sites. The solar wind stays southward during the whole time, and the short dispersion is observed before the long dispersion, which should not be the case if the long dispersion comes from another reconnection in the northern hemisphere. Another difference between these two dispersions is the variation of the maximum energy of electrons observed by FPI, which gradually decreases in the long dispersion and keeps constant in the short dispersion. Therefore, we consider that the parallel electron acceleration is occurring between the field lines of the short dispersion, which suggests that the field lines between the long dispersion and the separatrix are

inside the EDR. At the beginning of the long dispersion, the field lines should be outside the EDR and connected to the magnetosphere. The width of EDR in the magnetosheath side can be estimated based on in-situ observations. The distance observed by MMS from separatrix to the first reconnected field line (the beginning of the long dispersion) is 0.20 $d_{i,\ \mathrm{MSH}}$ or 9.86 $d_{e,\ \mathrm{MSH}}$, which is 6.33 $d_{e,\ \mathrm{MSH}}$ width in 2.94 RE upstream along the field line considering the convection motion of field line. The width of EDR observed in laboratory is 10–15d_e (Dong et al., 2012), which is consistent with the width of EDR we estimated based on MMS observation. The magnetic field (375 T) and plasma density (2.5–4.8×10^{19} cm^{-3}) is much larger in laboratory, but the Alfvén speed (V_A~720 km/s) is of the same order, The distance of 2.94 RE (183.63 $d_{i,\ \mathrm{Msh}}$) calculated in Figure 3 is the distance to the position where the electrons start to be frozen-in to the field line. Therefore, 2.94 RE only gives a lower limit of the real distance to the X-line in this case. The ion dispersion used to calculate this distance is also only seen for ions with a pitch angle between 0 to 45°, similar to the short dispersion of electrons. We cannot see the long dispersion of ions clearly because there are only three energy channels that cover the relevant ion energy range. However, we do observe the high energy ions from parallel to perpendicular directions (not shown). Considering the distance calculated in session 2.3, we believe that the electrons and ions close to the separatrix start to be magnetized at the same location. Based on these MMS1 observations, a schematic of MMS crossing the outflow region is shown in Figure 6 in the 00:56:45–00:57:40 UT interval on 1 January 2016.

The parallel electron beam with a narrow energy range (300–500 eV) appears outside of the electron edge. Fermi acceleration combined with the parallel potential close to the X-line is a possible candidate for the generation of the parallel electron beam. Inside the EDR, the magnetic field is determined by the motion of electrons (Lapenta et al., 2015). In this case, the reconnection electric field will contribute to the parallel potential, which points toward the X-line and will trap the electrons (Egedal et al., 2008); the parallel electric field caused by the parallel potential is marked as the orange line in Figure 7. Magnetosheath electrons with pitch angle close to 90° are trapped by the parallel potential and magnetic field close to the X-line, only when trapped electrons sufficiently energized through Fermi acceleration, shown as the green electron distribution inside the dashed line in Figure 7, can surpass the parallel potential, while the nontrapped magnetosheath electron distribution that crosses the X-line remains the same along the field line, shown as the purple electron distribution in Figure 7. The parallel potential blocks electrons with parallel energy between 140 to 230 eV and creates a slot between two dashed lines in Figure 5e. The illustration of this process is shown in Figure 7. This has also been observed by cluster and seen in PIC simulations inside the electron edge (Egedal et al., 2013), but never observed outside the electron edge. Lower band whistler mode waves and Langmuir waves have been observed before the electron beam (shown in Figure S1, see the supporting information for more details). Whistler mode waves can accelerate electrons in the parallel direction via Landau resonance ($\omega = k_{//} v_{//}$) to create a parallel electron beam, and Langmuir waves are excited by the electron beam. Wave-particle interaction might be another mechanism for the generation of the parallel electron beam (Li et al., 2018).

In summary, two types of electron dispersion have been observed in the separatrix region, which indicates that electrons and ions are not magnetized inside a thin layer close to the separatrix. Electrons for short dispersion should come from the EDR and the electrons for long dispersion come from the ion diffusion region. The width of EDR in the magnetosheath side, which is 6.33 $d_{e,\ \mathrm{MSH}}$, is estimated by MMS. The field lines are reconnected with the appearance of long dispersion. A parallel electron beam as a precursor of the electron edge is observed for the first time, which might be the result of the Fermi acceleration combined with a parallel potential drop and/or wave-particle interaction of the magnetosheath electrons close to the X-line.

Acknowledgments
MMS data are available at MMS Science Data Center (https://lasp.colorado.edu/mms/sdc/). Themis data are available at THEMIS Data Center (themis.ssl.berkeley.edu). We would like to thank Daniel J. Gershman from NASA Goddard Space Flight Center for checking the MMS FPI data. This work was supported by the National Natural Science Foundation of China (grants 41574157 and 41774153); Specialized Research Fund for State Key Laboratories, International Space Science Institute (ISSI); and the young scholar plan of Shandong University at Weihai (2017WHWLJH08). Shi-Chen Bai is supported by the State Scholarship Fund of Chinese Scholarship Council. Xiaogang Wang is funded by the National Natural Science Foundation of China (grants 41674165). I. J. R. is funded in part by STFC grant ST/N0007722/1 and NERC grants NE/L007495/1, NE/P017150/1, and NE/P017185/1.

References

Angelopoulos, V. (2008). The THEMIS mission. *Space Science Reviews*, *141*(1-4), 5–34. https://doi.org/10.1007/s11214-008-9336-1

Auster, H. U., Glassmeier, K. H., Magnes, W., Aydogar, O., Baumjohann, W., Constantinescu, D., et al. (2008). The THEMIS fluxgate magnetometer. *Space Science Reviews*, *141*(1-4), 235–264. https://doi.org/10.1007/s11214-008-9365-9

Birn, J., Drake, J. F., Shay, M. A., Rogers, B. N., Denton, R. E., Hesse, M., et al. (2001). Geospace Environmental Modeling (GEM) magnetic reconnection challenge. *Journal of Geophysical Research*, *106*(A3), 3715–3719. https://doi.org/10.1029/1999JA900449

Blake, J. B., Mauk, B. H., Baker, D. N., Carranza, P., Clemmons, J. H., Craft, J., et al. (2015). The Fly's Eye Energetic Particle Spectrometer (FEEPS) sensors for the Magnetospheric Multiscale (MMS) mission. *Space Science Reviews*, *199*(1-4), 309–329. https://doi.org/10.1007/s11214-015-0163-x

Broll, J. M., Fuselier, S. A., & Trattner, K. J. (2017). Locating dayside magnetopause reconnection with exhaust ion distributions. *Journal of Geophysical Research: Space Physics*, *122*, 5105–5113. https://doi.org/10.1002/2016JA023590

Burch, J. L., Moore, T. E., Torbert, R. B., & Giles, B. L. (2015). Magnetospheric Multiscale overview and science objectives. *Space Science Reviews*, *199*(1-4), 5–21. https://doi.org/10.1007/s11214-015-0164-9

Chen, L.-J., Hesse, M., Wang, S., Bessho, N., & Daughton, W. (2016). Electron energization and structure of the diffusion region during asymmetric reconnection. *Geophysical Research Letters*, *43*, 2405–2412. https://doi.org/10.1002/2016GL068243

Chen, L.-J., Pickett, J., Kintner, P., Franz, J., & Gurnett, D. (2005). On the width-amplitude inequality of electron phase space holes. *Journal of Geophysical Research*, *110*, A09211. https://doi.org/10.1029/2005JA011087

Dong, Q.-L., Wang, S. J., Lu, Q. M., Huang, C., Yuan, D. W., Liu, X., et al. (2012). Plasmoid ejection and secondary current sheet generation from magnetic reconnection in laser-plasma interaction. *Physical Review Letters*, *108*(21). https://doi.org/10.1103/physrevlett.108.215001

Egedal, J., Fox, W., Porkolab, M., Øieroset, M., Lin, R. P., Daughton, W., & Drake, J. F. (2008). Evidence and theory for trapped electrons in guide field magnetotail reconnection. *Journal of Geophysical Research*, *113*, A12207. https://doi.org/10.1029/2008JA013520

Egedal, J., Le, A., & Daughton, W. (2013). A review of pressure anisotropy caused by electron trapping in collisionless plasma, and its implications for magnetic reconnection. *Physics of Plasmas*, *20*(6). https://doi.org/10.1063/1.4811092

Ergun, R. E., Tucker, S., Westfall, J., Goodrich, K. A., Malaspina, D. M., Summers, D., et al. (2014). The axial double probe and fields signal processing for the MMS mission. *Space Science Reviews*, *199*(1-4), 167–188. https://doi.org/10.1007/s11214-014-0115-x

Fuselier, S. A., Trattner, K. J., Petrinec, S. M., Lavraud, B., & Mukherjee, J. (2018). Nonlobe reconnection at the Earth's magnetopause for northward IMF. *Journal of Geophysical Research: Space Physics*, *123*, 8275–8291. https://doi.org/10.1029/2018JA025435

Gosling, J. T., Thomsen, M. F., Bame, S. J., Onsager, T., & Russell, C. T. (1990). The electron edge of the low latitude boundary layer during accelerated flow events. *Geophysical Research Letters*, *17*(11), 1833–1836. https://doi.org/10.1029/GL017i011p01833

Graham, D. B., Khotyaintsev, Y. V., Norgren, C., Vaivads, A., André, M., Lindqvist, P. A., et al. (2016). Electron currents and heating in the ion diffusion region of asymmetric reconnection. *Geophysical Research Letters*, *43*, 4691–4700. https://doi.org/10.1002/2016GL068613

Hoshino, M., Hiraide, K., & Mukai, T. (2001). Strong electron heating and non-Maxwellian behavior in magnetic reconnection. *Earth, Planets and Space*, *53*(6), 627–634. https://doi.org/10.1186/bf03353282

Khotyaintsev, Y. V., Vaivads, A., Retinò, A., André, M., Owen, C. J., & Nilsson, H. (2006). Formation of inner structure of a reconnection separatrix region. *Physical Review Letters*, *97*(20). https://doi.org/10.1103/physrevlett.97.205003

Lapenta, G., Markidis, S., Divin, A., Newman, D., & Goldman, M. (2015). Separatrices: The crux of reconnection. *Journal of Plasma Physics*, *81*(1), 325810109. https://doi.org/10.1017/S0022377814000944

Lau, Y.-T., & Finn, J. M. (1990). Three-dimensional kinematic reconnection in the presence of field nulls and closed field lines. *The Astrophysical Journal*, *350*, 672. https://doi.org/10.1086/168419

Li, J., Bortnik, J., An, X., Li, W., Russell, C. T., Zhou, M., et al. (2018). Local excitation of whistler mode waves and associated Langmuir waves at dayside reconnection regions. *Geophysical Research Letters*, *45*, 8793–8802. https://doi.org/10.1029/2018GL078287

Lindqvist, P.-A., Olsson, G., Torbert, R. B., King, B., Granoff, M., Rau, D., et al. (2016). The spin-plane double probe electric field instrument for MMS. In *Magnetospheric Multiscale*, (pp. 137–165). Netherlands: Springer. https://doi.org/10.1007/978-94-024-0861-4_6

Mauk, B. H., Blake, J. B., Baker, D. N., Clemmons, J. H., Reeves, G. D., Spence, H. E., et al. (2016). The Energetic Particle Detector (EPD) investigation and the Energetic Ion Spectrometer (EIS) for the Magnetospheric Multiscale (MS) mission. *Space Science Reviews*, *199*(1-4), 471–514. https://doi.org/10.1007/s11214-014-0055-5

McFadden, J. P., Carlson, C. W., Larson, D., Ludlam, M., Abiad, R., Elliott, B., et al. (2008). The THEMIS ESA plasma instrument and in-flight calibration. *Space Science Reviews*, *141*(1-4), 277–302. https://doi.org/10.1007/s11214-008-9440-2

Mozer, F. S., Agapitov, O. A., Artemyev, A., Burch, J. L., Ergun, R. E., Giles, B. L., et al. (2016). Magnetospheric Multiscale satellite observations of parallel electron acceleration in magnetic field reconnection by Fermi reflection from time domain structures. *Physical Review Letters*, *116*(14). https://doi.org/10.1103/physrevlett.116.145101

Øieroset, M., Phan, T. D., Gosling, J. T., Fujimoto, M., & Angelopoulos, V. (2015). Electron and ion edges and the associated magnetic topology of the reconnecting magnetopause. *Journal of Geophysical Research: Space Physics*, *120*, 9294–9306. https://doi.org/10.1002/2015JA021580

Onsager, T. G., Thomsen, M. F., Gosling, J. T., & Bame, S. J. (1990). Electron distributions in the plasma sheet boundary layer: Time-of-flight effects. *Geophysical Research Letters*, *17*(11), 1837–1840. https://doi.org/10.1029/GL017i011p01837

Paschmann, G., Papamastorakis, I., Baumjohann, W., Sckopke, N., Carlson, C. W., Sonnerup, B. U. Ö., & Lühr, H. (1986). The magnetopause for large magnetic shear: AMPTE/IRM observations. *Journal of Geophysical Research*, *91*(A10), 11,099. https://doi.org/10.1029/ja091ia10p11099

Pollock, C., Moore, T., Jacques, A., Burch, J., Gliese, U., Saito, Y., et al. (2016). Fast plasma investigation for Magnetospheric Multiscale. *Space Science Reviews*, *199*(1-4), 331–406. https://doi.org/10.1007/s11214-016-0245-4

Retinò, A., Vaivads, A., André, M., Sahraoui, F., Khotyaintsev, Y., Pickett, J. S., et al. (2006). Structure of the separatrix region close to a magnetic reconnection X-line: Cluster observations. *Geophysical Research Letters*, *33*, L06101. https://doi.org/10.1029/2005GL024650

Russell, C. T., Anderson, B. J., Baumjohann, W., Bromund, K. R., Dearborn, D., Fischer, D., et al. (2016). The Magnetospheric Multiscale magnetometers. *Space Science Reviews*, *199*(1-4), 189–256. https://doi.org/10.1007/s11214-014-0057-3

Schwartz, S. J. (1998). Shock and discontinuity normals, mach numbers, and related parameters. ISSI Scientific Reports Series, 1, 249–270.

Trattner, K. J., Onsager, T. G., Petrinec, S. M., & Fuselier, S. A. (2015). Distinguishing between pulsed and continuous reconnection at the dayside magnetopause. *Journal of Geophysical Research: Space Physics*, *120*, 1684–1696. https://doi.org/10.1002/2014JA020713